Research Square

Preprints are preliminary reports that have not undergone peer review.
They should not be considered conclusive, used to inform clinical practice,
or referenced by the media as validated information.

IGF2BP3-Mediated Stabilization of LINC01671 Promotes LDHA-Dependent Glycolysis and Immune Evasion in Ovarian Clear Cell Carcinoma

Xiaonan Zhou
Fudan University Shanghai Cancer Center
Yifei Liu
Fudan University Shanghai Cancer Center
Jing Gao
Fudan University Shanghai Cancer Center
Ling Cui
Fudan University Shanghai Cancer Center
Hui Li
Fudan University Shanghai Cancer Center
Huijuan Ge
Fudan University Shanghai Cancer Center
Lin Yu
Fudan University Shanghai Cancer Center
Jiaojie Lv
Fudan University Shanghai Cancer Center
Ke Zuo
Fudan University Shanghai Cancer Center
Tian Tian
Fudan University Shanghai Cancer Center
Yue Wang
Fudan University Shanghai Cancer Center
Hui Sun
Fudan University Shanghai Cancer Center
Yufan Cheng
Fudan University Shanghai Cancer Center
Rui Bi
br_fdcc@163.com

Fudan University Shanghai Cancer Center

Article

Keywords: Ovarian Clear Cell Carcinoma, LINC01671, Aerobic Glycolysis, Immune Evasion, RNA-Binding Protein

Posted Date: September 23rd, 2026

DOI: https://doi.org/10.21203/rs.3.rs-10858771/v1

License: This work is licensed under a Creative Commons Attribution 4.0 International License. Read Full License

Additional Declarations: No competing interests reported.

Abstract

Ovarian clear cell carcinoma (OCCC) is a highly chemoresistant subtype of ovarian cancer with limited therapeutic options, while the mechanisms underlying metabolic reprogramming and immune evasion remain incompletely understood. In this study, integrative transcriptomic and metabolomic analyses identified the long non-coding RNA LINC01671 as markedly upregulated in OCCC and associated with poor clinical outcomes. Functional experiments demonstrated that LINC01671 promotes tumor growth, invasion, and aerobic glycolysis both in vitro and in vivo. Mechanistically, LINC01671 interacts with the RNA-binding protein IGF2BP3, which enhances its stability and facilitates upregulation of lactate dehydrogenase A (LDHA), thereby driving glycolytic reprogramming. Moreover, LINC01671 impaired MHC I–mediated antigen presentation and suppressed $CD8^+$ T cell cytotoxicity, accompanied by reduced secretion of Granzyme B, IFN-γ, and Perforin, indicating a role in immune escape. Importantly, genetic depletion of LINC01671 or LDHA reversed these oncogenic and immunosuppressive phenotypes and sensitized tumor cells to T cell–mediated killing. Collectively, these findings identify an IGF2BP3–LINC01671–LDHA regulatory axis linking metabolic reprogramming to immune suppression and provide mechanistic insight into OCCC progression.

Background

Ovarian cancer (OV) remains the most lethal gynecological malignancy, with a 5-year survival rate of only ~ 30%[1]. While high-grade serous carcinoma is the most prevalent subtype, ovarian clear cell carcinoma (OCCC) has emerged as a distinct clinical and molecular entity with a disproportionately high incidence in East Asian populations, reaching up to 30% in Japan compared to 10–12% in North America[2]. Unlike other subtypes, OCCC is etiologically linked to endometriosis and characterized by a high frequency of mutations in ARID1A and PIK3CA[3, 4]. Although early-stage OCCC patients typically have a favorable prognosis following optimal cytoreductive surgery, advanced or recurrent cases frequently exhibit profound resistance to platinum-based chemotherapy, resulting in limited therapeutic options and poor clinical outcomes[5].

A hallmark of cancer progression is metabolic reprogramming, particularly the "Warburg effect"[6]. Accumulating evidence indicates that dysregulated glycolytic pathways not only provide biosynthetic intermediates and ATP but also contribute to chemoresistance and tumor aggressiveness[7, 8]. However, the regulatory networks governing metabolic remodeling in OCCC remain incompletely understood.

Long non-coding RNAs (lncRNAs) have emerged as critical regulators of gene expression and tumor biology[9, 10]. Through interactions with RNA-binding proteins (RBPs), lncRNAs modulate mRNA stability[11], translation[12], and subcellular localization[13], thereby influencing diverse oncogenic processes[14], including metabolic adaptation[15]. Despite growing recognition of lncRNA–RBP regulatory axes in cancer, their functional relevance in OCCC metabolism has not been fully elucidated.

Although LINC01671 has been linked to genomic instability in lung adenocarcinoma[16, 17] and purine metabolism in renal cell carcinoma[18]; the underlying mechanisms remain unclear, and its role in OCCC

has not been investigated. In this study, we identify LINC01671 as a transcript specifically upregulated in OCCC that correlates with poor clinical outcomes. Integrating transcriptomic and untargeted metabolomic profiling, we demonstrate that LINC01671 acts as a master regulator of glycolytic remodeling. Mechanistically, LINC01671 physically interacts with the RBP IGF2BP3, which enhances the stability of LINC01671 and promotes LDHA-mediated glycolysis. This sustains a pro-glycolytic program that drives the malignant phenotype of OCCC. Our findings define the IGF2BP3/LINC01671/LDHA axis as a critical metabolic driver and a promising therapeutic target for OCCC.

Methods

Bioinformatic analyses

Online GSE226870 dataset was analyzed. Differentially-expressed lncRNAs (DELs) between three primary OCCC tissues and normal ovary samples and differentially-expressed genes between the NC group and LINC01671 knockdown group were analyzed using the limma R package. We performed the Gene Ontology (GO) and Kyoto Encyclopedia of Genes and Genomes (KEGG) analysis and gene set variation analysis (GSVA) analysis to explore the potential mechanisms through which LINC01671 regulates tumor progression.

Patient and tissue samples

To perform RNA sequencing, we used primary OCCC tissues and corresponding normal ovary samples from three patients who did not receive any neoadjuvant treatment before surgery. We also extracted tissue RNA from tumor tissues of 45 patients diagnosed with OCCC who underwent surgical resection between 2000 and 2021, along with 8 normal ovarian surface epithelium (OSE) samples used as controls. Collected tissues were stored in RNA Keeper Tissue Stabilizer (Vazyme, Nanjing, China) at −80°C. Supplementary Table 1 summarizes the clinical information of these patients. Our study was approved by the Ethics Committee on Scientific Research of Fudan University Shanghai Cancer Center, and all the individuals involved in this study provided written informed consent for the use of clinical samples in medical research. All methods were performed in accordance with the relevant guidelines and regulations.

Cell culture and transfection

Human embryonic kidney cell line (HEK-293T), human OCCC cell lines (TOV21G and OVISE) and normal ovarian epithelial cell lines (IOSE80) were obtained from the Chinese Academy of Cell Collection (Shanghai, China), and cultured in a humidified conditions at 37°C with 5% CO2. HEK-293T, TOV21G and OVISE cells were cultivated in DMEM (DMEM, Shanghai Yuanpei Company) with fetal bovine serum (FBS) and 1% penicillin/streptomycin (PS).

When the cell fusion degree reached 60–70%, short hairpin RNAs (shRNAs) and small interfering RNAs (siRNAs) (Tsingke Biotech, Beijing, China) targeting LINC01671, IGF2BP3 and LDHA as well as overexpression plasmids (Shanghai Fanxu Technology) and an empty vector (EV) were transfected into OCCC cells by Liposomal 2000 Transfection Reagent (Yeasen, Shanghai, China).

HEK-293T cells were transfected with the knockdown/overexpressed plasmids, psPAX2, and pMD2.G, using a transfection reagent. After 48 h, the culture medium of HEK-293T cells (containing lentivirus particles encapsulating knockdown/overexpression constructs) was harvested, filtered using a percolator whose bore diameter is 0.45 μm (Millipore, USA), and applied to transfect OCCC cells to knock down or overexpress LINC01671, IGF2BP3 and LDHA. Stable cell lines were selected using a culture medium containing 5μg/mL puromycin. Supplementary Table 2 summarized the sequences of shRNAs and siRNAs.

RNA extraction and real-time quantitative polymerase chain reaction (RT–qPCR)

Tissues fixed in RNA Keeper Tissue Stabilizer were ground to powder with liquid nitrogen. We extracted RNA with Total RNA Extraction Reagent (Invitrogen, USA) and reverse transcribed it into cDNA with the PrimeScript RT reagent Kit (TaKaRa, Japan). Nuclear and Cytoplasmic Protein Extraction Kit (Beyotime Biotech, Shanghai, China) was applied to find out the subcellular localization of LINC01671. RT–qPCR analysis was performed to detect the expression of relevant genes using the SYBR Green PCR Kit (Taraka, Japan) and ABI 7900 real-time PCR Detection System (Applied Biosystems, USA). β-actin and U6 served as the internal reference. All the experiments were performed in triplicate, and primers are shown in Supplementary Table 3.

Cell proliferation and invasion assay

For the CCK-8 assay, 1,000 treated OCCC cells were seeded into each well of 96-well plates. CCK-8 reagent (YEASEN, China) was then added to each well, followed by incubation in the dark at 37°C for 2 h. Absorbance was measured at 24-h intervals from day 1 to day 4. Cell proliferative capacity was further assessed using a colony formation assay. Briefly, 1,000 treated OCCC cells were seeded in 1.5 ml of complete culture medium per well. All independent experiments were conducted with identical incubation times. After approximately two weeks, cells were fixed with 4% paraformaldehyde (ServiceBio, China) for 30 min and stained with 1% crystal violet (YEASEN, China). Cell invasive ability was evaluated using a Transwell invasion assay. Diluted Matrigel (BD Biosciences, USA) was added to the upper chambers, while 600 μl of complete medium was placed in the lower chambers. Subsequently, 200 μl of cell suspension containing 3×10^4 cells was seeded into each upper chamber and incubated for 48 h. Invaded cells were then fixed, stained, photographed, and quantified after removal of non-invaded cells from the upper surface of the membrane. All experiments were performed in triplicate.

Western blotting

Proteins were extracted from human OCCC cells by lysis in RIPA buffer on ice for 10 min, followed by further disruption using ultrasonic waves. Protein concentrations were determined using the Pierce™ BCA Protein Assay Kit (Thermo Fisher Scientific). Samples were adjusted with 5× loading buffer and additional RIPA buffer according to protein concentration, and denatured at 95°C. Equal amounts of protein were resolved by SDS-PAGE and transferred onto PVDF membranes (0.45 μm; Millipore, Germany). Transfer conditions, including voltage, current, and duration, were optimized based on the molecular weight of the target protein. Membranes were blocked with 5% milk and incubated with primary antibodies for at least 10 h at 4°C with gentle agitation, followed by incubation with secondary antibodies for 1 h at room temperature. Protein detection was performed using a chemiluminescence imaging system. All antibodies used in this study are listed in Supplementary Table 4.

Fluorescence in situ hybridization (FISH) and immunofluorescence (IF) assays

Subcellular localization of LINC01671 was determined using a FISH Kit (GenePharma, Shanghai, China) following the manufacturer's protocol. Cy3-labeled LINC01671-specific probes, 18S and corresponding negative controls (NC) were designed and synthesized by GenePharma; detailed probe sequences are provided in Supplementary Table 5.

For co-localization analysis, the FISH assay was followed by immunofluorescence staining. Cells were incubated overnight at 4°C with a primary antibody against IGF2BP3 (14642-1-AP, Proteintech; 1:50 dilution) and LDHA (19987-1-AP, Proteintech; 1:100 dilution). Subsequently, cells were treated with an Alexa Fluor 488-conjugated goat anti-rabbit IgG secondary antibody (GB25303, Servicebio; 1:250 dilution) for 1 h at room temperature. Nuclei were counterstained with DAPI for 10 min. All images were acquired using a laser-scanning confocal microscope to resolve the spatial distribution of LINC01671 and IGF2BP3 within the OCCC cells.

RNA pull-down and RNA immunoprecipitation (RIP) assays

For the RNA pull-down assay, the Pierce™ Magnetic RNA-Protein Pull-Down Kit (2164, Thermo Fisher Scientific, USA) was used following the manufacturer's instructions. Briefly, biotin-labeled RNA was incubated with streptavidin magnetic beads under agitation for 30 min at room temperature. The RNA-bound beads were subsequently incubated with cell lysates for 60 min at 4°C. RNA–protein complexes were separated by 10% SDS-PAGE and visualized by silver staining. For RNA immunoprecipitation (RIP) assays, the Magna RIP™ RNA-Binding Protein Immunoprecipitation Kit (17–700, Millipore, USA) was applied according to the manufacturer's protocol. Protein A/G beads were pre-incubated with 3 μg of anti-IGF2BP3 (14642-1-AP, Proteintech; 1:50), anti-LDHA (19987-1-AP, Proteintech; 1:100), or control IgG for 30 min at room temperature. Cell lysates were then incubated with the antibody–bead complexes

overnight at 4°C. Proteinase K treatment was performed to digest proteins, followed by RNA extraction, purification, reverse transcription, and quantitative RT-PCR analysis.

Glucose consumption, ATP production, and lactate production

Glycolytic activity was evaluated by quantifying glucose uptake, intracellular ATP levels, and lactate secretion. Glucose consumption was measured using a Glucose Uptake Assay Kit (Dojindo, Japan) according to the manufacturer's instructions. Intracellular ATP concentrations were determined using an Enhanced ATP Assay Kit (Beyotime, China), based on the luciferase-catalyzed conversion of luciferin; the resulting bioluminescence was quantified using a multimode microplate reader. Lactate production in the conditioned media was assessed using an L-Lactic Acid (LA) Colorimetric Assay Kit (Elabscience, China) via enzymatic oxidation and subsequent colorimetric detection.

To ensure comparability across experimental groups, all metabolic parameters were normalized to total protein concentrations, as determined by the BCA assay. Each experiment was conducted in triplicate across at least three independent biological replicates.

RNA stability assay

TOV21G and OVISE cells with IGF2BP3 overexpression or knockdown, as well as corresponding vector controls, were seeded in six-well plates and treated with actinomycin D (5 μg/ml; Abclonal). Total RNA was isolated at the indicated time points, and LINC01671 mRNA levels were quantified by qRT–PCR.

Flow cytometry

Flow cytometry was performed according to the manufacturers' instructions. Apoptosis was assessed using the Annexin V-PE/7-AAD Apoptosis Detection Kit (A213-01, Vazyme, Nanjing, China).

To evaluate antigen presentation machinery, tumor cells were harvested and stained for surface markers, including FITC-conjugated anti-human HLA-ABC (Clone W6/32, BioLegend) and PE/Cyanine7-conjugated anti-human HLA-DR (Clone L243, BioLegend).

For CD8 + T cell functional assays, peripheral blood mononuclear cells (PBMCs) were isolated from human peripheral blood, and CD8 + T cells were subsequently purified and activated. Activated CD8 + T cells were then co-cultured with tumor cells, and the expression of effector molecules, including granzyme B (GzmB), interferon-γ (IFN-γ), and perforin, was analyzed by flow cytometry.

For surface staining, cells were incubated with fluorophore-conjugated antibodies, including FITC anti-human CD8 (Clone SK1, BioLegend). For intracellular staining, cells were fixed and permeabilized using Intracellular Staining Perm Wash Buffer (Cat#421002, BioLegend), followed by staining with PE/Cyanine5 anti-human/mouse Granzyme B Recombinant Antibody (Clone QA16A02, BioLegend),

Brilliant Violet 421™ anti-human IFN-γ Antibody (Clone 4S.B3, BioLegend) and APC anti-human Perforin Antibody (clone δG9, BioLegend).

Gating strategies rely on forward vs. scatter characteristics, followed by single-cell gating for viable cells. The data were acquired and subsequent analysis was conducted using FlowJo software.

Untargeted metabolomic analysis

To characterize the global metabolic alterations induced by LINC01671 knockdown, untargeted metabolomic profiling (Metabo-Profile, Shanghai, China) was performed on TOV21G cells (n = 4 per group). Cells were washed 2–3 times with ice-cold PBS to remove residual medium and detached using 1× trypsin at 37°C for 5 min. Digestion was terminated with complete medium, and cells were collected by centrifugation at 200–1,000g for 10 min at 4°C. Cell pellets were washed 2–3 additional times with cold PBS and resuspended for counting. A total of 5.0×10^6 to 1.0×10^7 cells were aliquoted into 1.5 ml tubes, centrifuged at 4°C, and supernatants were carefully removed to minimize buffer interference with mass spectrometry. Cell pellets were rapidly quenched in liquid nitrogen and stored at − 80°C until analysis. Identified metabolites are listed in Supplementary Table 6.

In vivo xenograft experiments

All animal procedures were approved by the Committee on the Ethics of Animal Experiments of Fudan University and conducted in strict accordance with the institutional guidelines for the care and use of laboratory animals. Five-week-old female athymic BALB/c nude mice (Vital River Laboratory, Beijing, China) were maintained under specific-pathogen-free (SPF) conditions, with a 12-h light/dark cycle, a temperature range of 22–28°C, and 50–70% humidity.

For the subcutaneous xenograft model, mice were randomly assigned to experimental groups (n = 5 per group). A total of 5 x 10^6 TOV21G cells, stably transduced with either LINC01671-knockdown (sh-LINC01671), LINC01671-overexpression (OE-LINC01671), or their respective negative controls (sh-NC or Vector), were suspended in 100 ul PBS and injected subcutaneously into the right flank of each mouse.

The tumor volumes were calculated every 3 days (V = 0.5 × D × d2 (V, volume; D, longitudinal diameter; d, latitudinal diameter)).To adhere to humane endpoints, mice were euthanized when the tumor volume approached 1,000 mm^3. Following sacrifice, the tumors were surgically excised, photographed for further analysis.

Statistical analysis

The data downloaded from the GSE database was processed and analysed by the R software (version 4.1.2). Statistical analysis and visualization were conducted using the R software and GraphPad Prism 8. Two-sided Student's t-test was used to analyze differences between two groups, while one-way ANOVA was used to compare statistics among three or more groups. The Tukey test, Bonferroni test, or Dunnett test were used for post multiple comparisons between groups. We used the $\chi 2$ test and Fisher's exact test to analyze the relationship between LINC01671 expression and clinicopathologic features.

Pearson’s correlation analysis was used to explore correlations between the groups. Kaplan–Meier analysis and a log-rank test were performed for survival analysis. The accuracy and stability of the risk model were evaluated by receiver operating characteristic (ROC) curves and area under the curve (AUC) values. P value < 0.05 was considered to be statistically significant. All experiments were performed in triplicates.

Results

3.1 Characterization of LINC01671 in OCCC

To identify long non-coding RNAs (lncRNAs) driving OCCC pathogenesis, we performed RNA sequencing (RNA-seq) on three pairs of OCCC and normal ovarian tissues (FUSCC cohort). To ensure robustness, we integrated these findings with transcriptomic data from the GTEx (normal ovary) and GEO (GSE226870) databases (Figure. 1A). Using a cutoff of |fold change| > 2 and P < 0.05, we identified differentially expressed genes in each dataset and obtained 59 overlapping candidates by intersection analysis (Figure. 1B).

Given the distinct histological and clinical characteristics of OCCC, which is associated with poorer outcomes in advanced stages compared with other ovarian cancer subtypes[19], we further sought to identify lncRNAs specifically enriched in OCCC. Validation using the independent dataset GSE189553 demonstrated that LINC01671 was selectively upregulated in OCCC compared with high-grade serous carcinoma and endometrioid carcinoma (Figure. 1C).

We next validated the clinical relevance of LINC01671 in an expanded FUSCC cohort (n = 45). LINC01671 was significantly upregulated in OCCC tissues compared to normal ovarian surface epithelium (Figure. 1D). Based on LINC01671 expression levels, patients were stratified into LINC01671-high (n = 23) and LINC01671-low (n = 22) groups. Kaplan–Meier analysis revealed that patients with high LINC01671 expression exhibited significantly worse overall survival (OS) and reduced 5-year overall survival compared with those in the low-expression group (Figure. 1E). Univariate and multivariate Cox proportional hazards analyses identified LINC01671 expression as an independent prognostic factor for OCCC (HR = 10.136, p = 0.031), alongside FIGO stage (Figure. S1A). Notably, time-dependent ROC analysis demonstrated high predictive accuracy for LINC01671, with AUC values of 0.756, 0.705, and 0.686 at 1, 3, and 5 years, respectively (Figure. S1B).

According to the NCBI database, LINC01671 is located on the long arm of chromosome 21 and has a single annotated transcript, LINC01671-201 (Figure. S1C). Coding potential analysis using Ensembl annotation and the CPC2 algorithm indicated that LINC01671 lacks protein-coding capacity (Figure. S1D). Consistent with our clinical findings, LINC01671 expression was markedly elevated in OCCC cell lines (TOV21G and OVISE, which have been molecularly classified as clear cell carcinoma models) compared to normal ovarian epithelial cells (Figure. 1F). These two cell lines were therefore selected for subsequent loss- and gain-of-function experiments. Subcellular fractionation and fluorescence in situ

hybridization (FISH) assays demonstrated that LINC01671 was distributed in both the cytoplasm and nucleus of OCCC cells (Figure. 1G, H), suggesting potential multifunctional regulatory roles.

3.2 LINC01671 promotes the proliferation and invasion of OCCC cells in vitro and in vivo

To elucidate the functional role of LINC01671 in OCCC progression, we established stable knockdown and overexpression models in TOV21G and OVISE cell lines, confirming high transfection efficiency via qRT-PCR (Figure. S2A, B). Functional assays consistently demonstrated that silencing LINC01671 significantly suppressed cell proliferation, as assessed by both colony formation and CCK-8 assays, whereas LINC01671 overexpression markedly enhanced proliferative capacity in both cell lines (Figure. 2A–D). Transwell invasion assays revealed that LINC01671 depletion substantially impaired the invasive potential of TOV21G and OVISE cells, while enforced LINC01671 expression promoted invasion (Figure. 2E, F). Apoptosis analyses further showed that knockdown of LINC01671 significantly increased apoptotic cell populations, whereas LINC01671 overexpression exerted a protective effect against apoptosis in both OCCC cell lines (Figure. 2G–J). Collectively, these in vitro findings identify LINC01671 as a potent regulator of the malignant phenotype in OCCC.

To validate these observations in vivo, we established a mouse subcutaneous xenograft model. Consistent with the in vitro results, LINC01671 knockdown significantly inhibited tumor growth, as evidenced by reduced tumor volume (Figure. 2K,L). Conversely, LINC01671 overexpression markedly accelerated tumor growth in vivo (Figure. 2M,N). Together, these data demonstrate that LINC01671 acts as a potent driver of OCCC tumor growth both in vitro and in vivo.

3.3 LINC01671 regulates aerobic glycolysis in OCCC

To explore downstream pathways associated with LINC01671, we first analyzed the GSE226870 dataset and performed Pearson correlation analysis to identify genes most strongly correlated with LINC01671 expression ($P < 0.05$, $r > 0.5$). Functional enrichment (GO/KEGG) and Gene Set Variation Analysis (GSVA) of the top 200 LINC01671-correlated genes highlighted a predominant association with metabolic pathways, specifically central carbon metabolism in cancer and sphingolipid biosynthesis (Figure. 3A–C, Figure. S3A, B).

To functionally validate these associations, we performed RNA sequencing in TOV21G cells with stable LINC01671 knockdown (sh-LINC01671, n = 6) and control cells (sh-NC, n = 3). Differential expression analysis ($|log_2FC| > 1$, $P < 0.05$) identified 232 upregulated and 126 downregulated transcripts (Figure. 3D, E). Downregulated genes were significantly enriched in the cell cycle, DNA repair, and glycolytic pathways, including HIF-1 signaling (Figure. 3F). Conversely, upregulated genes were primarily associated with antigen processing and MHC-II presentation (Figure. 3G, H). Consistent with this, LINC01671 depletion markedly increased HLA-DMA and HLA-DRB1 expression. Furthermore, different cell subsets in the microenvironment suggested that LINC01671 knockdown correlates with an increased signature of T cells, cytotoxic lymphocytes, and monocytic lineages (Figure. S3D, E), suggesting that LINC01671 may facilitate immune evasion in OCCC.

To further interrogate the metabolic consequences of LINC01671 regulation, we performed pathway enrichment analysis of all differentially expressed genes using MetaboAnalyst, which identified glycolysis as a major pathway impacted by LINC01671 (Figure. 3I). We then conducted targeted metabolomic profiling (Metabolon Q300) to validate metabolic alterations induced by LINC01671 knockdown. Principal component analysis and permutation testing revealed distinct metabolic profiles between sh-NC (n = 4) and sh-LINC01671 (n = 4) cells (Figure. S3F,G), indicating extensive metabolic reprogramming. Among 177 detected metabolites, 71 were significantly depleted following LINC01671 knockdown, predominantly involving organic acids and carbohydrates (Figure. 3J–M). Metabolic pathway enrichment further confirmed the Warburg effect as the functional nexus, aligning with the central carbon metabolism and glycolytic pathways highlighted by previous database screening and RNA-seq analysis (Figure. 3N). Specifically, LINC01671 silencing led to a substantial reduction in essential glycolytic intermediates, including glucose-6-phosphate, fructose-6-phosphate, pyruvate, and lactate (Figure. 3O). Collectively, these data establish LINC01671 as a critical metabolic driver that promotes glycolytic flux.

3.4 LINC01671 promotes glycolysis by interacting with and regulating LDHA

To elucidate the mechanism by which LINC01671 modulates glycolysis, we performed a correlation analysis between LINC01671 and glycolytic gene expression profiles from transcriptome sequencing data. Among all candidates, LDHA exhibited the strongest positive correlation with LINC01671 expression (cor = 0.58; Figure. 4A). Consistently, transcriptomic analysis of LINC01671-knockdown cells revealed that LDHA was the most significantly downregulated glycolytic gene (Figure. S4A-G). The spatial relationship between these two molecules was further supported by co-immunostaining, which confirmed the colocalization of LINC01671 and LDHA in OCCC cells (Figure. 4B).

We next validated these findings experimentally. RT-qPCR analysis showed that LINC01671 knockdown led to a marked reduction in most glycolytic genes, except PGM1, aligning with our transcriptomic data (Figure. 4C). Conversely, LINC01671 overexpression broadly upregulated these genes (Figure. 4D). At the protein level, LDHA expression was significantly reduced following LINC01671 knockdown and elevated upon LINC01671 overexpression (Figure. 4E).

Given the strong association between LINC01671 and LDHA, we next investigated whether LINC01671 directly regulates LDHA. RNA pulldown followed by western blotting and RIP–qPCR assays confirmed that LINC01671 interacted with LDHA (Figure. 4F,G). Functionally, glucose uptake, ATP production, and lactate production assays showed that LINC01671 knockdown significantly suppressed glycolytic activity in TOV21G and OVISE cells, whereas LINC01671 overexpression enhanced glucose uptake, ATP generation, and lactate production (Figure. 4H–M).

Collectively, these results indicate that LINC01671 promotes glycolysis in OCCC cells through direct regulation of LDHA.

3.5 LINC01671 impairs antigen presentation and CD8 + T cell cytotoxicity in OCCC

Glycolysis is known to create an acidic tumor microenvironment, which inhibits antigen presentation and the cytotoxic function of immune cells[20, 21]. Integrated transcriptomic profiling identified LINC01671 as a putative regulator of antigen processing and presentation (Figure. 3H, S3D), with its expression levels negatively correlated with CD8 + T cell and cytotoxic lymphocyte signatures (Figure. S3E). To mechanistically link LINC01671 to immune evasion, we assessed the surface expression of MHC molecules. Flow cytometric analysis of MHC I and II expression in tumor cells revealed that, compared to the sh-NC group, MHC I expression was significantly upregulated in the LINC01671 knockdown group, while MHC II expression remained unchanged (Figure. 5A).

CD8 + T cells play a crucial role in tumor cell killing, with effector proteins such as interferon-γ (IFN-γ), granzyme B (GzmB), and perforin directly contributing to lymphocyte-mediated cytotoxicity. We examined the impact of LINC01671 interference on T cell effector functions. Co-culture assays revealed that LINC01671 interference markedly increased the proportions of GzmB-, IFN-γ-, and perforin-positive T cells compared to sh-NC controls (Figure. 5B–D). Similar results were observed in the OVISE cell line (Figure. S5A-D). Data from MHC expression and analysis of markers critical to T cell cytotoxic potential consistently supported the conclusion that LINC01671 influences tumor antigen presentation and CD8 + T cell function.

3.6 LINC01671 promotes OCCC proliferation, migration and aerobic glycolysis in an LDHA-dependent manner

To define the functional role of LDHA in OCCC, we modulated its expression in TOV21G and OVISE cells, with transfection efficiencies validated by western blot (Figure. S6A). LDHA silencing markedly suppressed cell proliferation and invasion, whereas LDHA overexpression significantly enhanced the proliferative and invasive capacities of both TOV21G and OVISE cells (Figure. 6A–D). Consistently, glucose uptake, ATP production, and lactate production assays demonstrated LDHA silencing markedly inhibited glucose uptake, ATP production, and lactate formation. Conversely, LDHA overexpression robustly enhanced these glycolytic parameters (Figure. 6E–J). Although antigen processing and presentation by tumor cells are critical for immune recognition, the cytotoxic activity of CD8 + T cells ultimately mediates tumor cell killing. We therefore examined the impact of LDHA on CD8 + T cell effector function. In OCCC cell lines, LDHA knockdown significantly increased the proportion of IFN-γ–positive T cells in TOV21G cells compared with the sh-NC group, whereas no significant change was observed in OVISE cells. In contrast, the proportion of GzmB-positive T cells did not differ between knockdown and control groups in either OCCC cell line (Figure. S6B, C).

We next performed rescue experiments to determine whether LINC01671 exerts its oncogenic effects through LDHA. We silenced LDHA in LINC01671-overexpressing cells, confirming the knockdown efficiency via western blot (Figure. S6D). Functional recovery assays demonstrated that the LINC01671-mediated increases in cell proliferation (Figure. S6E, F) and invasive capacity (Figure. S6G, H) were significantly attenuated upon LDHA depletion.

Collectively, LDHA is required for LINC01671-driven malignant phenotypes in OCCC cells.

3.7 IGF2BP3 interacts with and stabilizes LINC01671 in OCCC cells

Given the predominantly cytoplasmic localization of LINC01671 (Figure. 1G,H), we hypothesized that it may exert its oncogenic functions through physical interactions with specific RNA-binding proteins (RBPs)[22]. To identify these partners, we performed RNA-pulldown assays using biotinylated LINC01671 probes, followed by mass spectrometry, which identified 24 proteins specifically associated with the LINC01671 sense strand (Figure. 7A; Figure. S7A).

Simultaneously, we found that both the sense and antisense strands of LINC01671 could bind to IGF2BP3 using RBPsuite(http://www.csbio.sjtu.edu.cn/bioinf/RBPsuite/) (Figure. S7B). Thus, we performed western blotting using an anti-IGF2BP3 antibody to verify that IGF2BP3 existed in eluted samples of LINC01671 sense and antisense stands obtained after the pull-down assay (Figure. 7B). On the other hand, RIP assays results indicated that LINC01671 was dominantly enriched in the IP-RNA of IGF2BP3 compared with IgG (Figure. 7C). Concurrently, FISH and IF assay results showed that LINC01671 and IGF2BP3 were co-localized in the cytoplasm of OCCC cells (Figure. 7D). In summary, these results suggested that LINC01671 was specifically bound to IGF2BP3.

We next investigated whether LINC01671 regulates IGF2BP3 expression in OCCC cells. Neither knockdown nor overexpression of LINC01671 altered IGF2BP3 mRNA or protein levels in TOV21G and OVISE cells, indicating that IGF2BP3 is not transcriptionally or translationally regulated by LINC01671 (Figure. 7E-G). In contrast, modulation of IGF2BP3 expression significantly affected LINC01671 RNA abundance (Figure. 7H,J,L,N). Given that IGF2BP3 has been reported to enhance the stability of long non-coding RNAs[23], we performed mRNA stability assays. IGF2BP3 overexpression markedly prolonged the half-life of LINC01671, whereas IGF2BP3 silencing accelerated LINC01671 decay in OCCC cells (Figure. 7I,K,M,O). These findings indicate that IGF2BP3 stabilizes LINC01671 post-transcriptionally, thereby sustaining its oncogenic function in OCCC.

3.8 IGF2BP3/LINC01671/LDHA axis regulates OCCC progression

To investigate whether IGF2BP3 influences the LINC01671/LDHA axis, we first examined its regulatory effect on LDHA. Knockdown of IGF2BP3 markedly decreased both LDHA mRNA and protein levels, whereas IGF2BP3 overexpression led to a significant upregulation of LDHA expression in TOV21G and OVISE cells (Figure. 8A–C). We next assessed the functional role of IGF2BP3 in OCCC progression. IGF2BP3 silencing significantly suppressed cell proliferation and invasion, whereas its overexpression exerted the opposite effects in both TOV21G and OVISE cells (Figure. 8D–G). We next assessed the impact of IGF2BP3 on CD8 + T cell effector function. In TOV21G cells, IGF2BP3 knockdown significantly increased the proportions of GzmB- and IFN-γ–positive T cells compared with the sh-NC group. In contrast, no significant differences in these effector proteins were observed between the knockdown and control groups in OVISE cells (Figure. S8A, B).

We next performed functional rescue experiments to determine if IGF2BP3 exerts its effects through LINC01671 (Figure. 8H). Notably, the enhancement in cell proliferation and invasion mediated by

IGF2BP3 overexpression was significantly attenuated by the concomitant silencing of LINC01671 (Figure. 8I,J). These results establish that LINC01671 is a critical downstream mediator of IGF2BP3-induced oncogenesis, suggesting that the IGF2BP3/LINC01671/LDHA signaling axis plays a pivotal role in the progression of OCCC.

Discussion

Metabolic reprogramming has re-emerged as a central vulnerability in cancer therapy[24, 25]. Although cytoreductive surgery and platinum-based chemotherapy remain the standard of care for OCCC, resistance is common and therapeutic options are limited[26]. Targeting glycolytic enzymes, including LDHA, has shown encouraging preclinical activity[27], yet clinical translation has been hindered by metabolic plasticity and the lack of precise patient stratification[28]. Our findings position the IGF2BP3/LINC01671/LDHA axis as an upstream regulatory node of glycolysis in OCCC, suggesting that interference at the level of post-transcriptional control may achieve more durable metabolic suppression than direct enzymatic inhibition alone. Therapeutically, this raises the possibility of combining glycolysis inhibitors with agents targeting RNA–protein interactions to overcome chemoresistance in OCCC[29].

Through integrative analysis of sequencing data and publicly available datasets, we identified LINC01671 as a lncRNA that is specifically upregulated in OCCC. Elevated LINC01671 expression was significantly associated with unfavorable clinical outcomes in patients with OCCC. Functional studies performed both in vitro and in vivo demonstrated that LINC01671 promotes tumor growth and progression.

To further delineate its mechanistic role, we conducted transcriptomic and metabolomic profiling following LINC01671 knockdown. Integrated multi-omics analyses revealed that depletion of LINC01671 markedly impaired glycolytic activity, impairs antigen presentation and CD8 + T cell cytotoxicity in OCCC cells. Notably, this metabolic alteration was accompanied by a significant reduction in LDHA expression, suggesting that LINC01671 sustains glycolytic flux, at least in part, through the regulation of LDHA.

The "Warburg effect"—characterized by persistent aerobic glycolysis—is a defining hallmark of OCCC, fueling its rapid proliferation and profound chemoresistance[30]. LDHA occupies a pivotal position at the terminal step of aerobic glycolysis, catalyzing the conversion of pyruvate to lactate while regenerating NAD^+ to sustain continuous glycolytic flux[31]. Beyond its metabolic function, LDHA contributes to tumor progression through multiple interconnected mechanisms. Elevated lactate production acidifies the tumor microenvironment, promoting extracellular matrix remodeling[32], immune evasion[33], and angiogenesis[34]. In this context, accumulating lactate has been shown to impair $CD8^+$ T-cell effector functions and promote immune evasion within the tumor microenvironment[35]. Although our data demonstrate that LINC01671-mediated glycolytic activation is accompanied by impaired antigen presentation and reduced T-cell cytotoxicity, the precise metabolic signals linking these processes remain to be clarified. Importantly, accumulating evidence suggests that LDHA hyperactivation is not solely a downstream consequence of oncogenic signaling but may function as an adaptive safeguard

that buffers metabolic stress and facilitates therapeutic resistance[36]. Our study identifies LINC01671 as a master post-transcriptional regulator that sustains this metabolic program. By integrating transcriptomic and untargeted metabolomic profiling, we demonstrate that LINC01671 specifically amplifies glycolytic flux by enhancing the expression of LDHA, the rate-limiting enzyme responsible for converting pyruvate to lactate. Experimentally, we observed that LINC01671 depletion significantly blunts glucose consumption and lactate production, effectively "starving" the cells of the energetic and biosynthetic intermediates required for malignancy.

A central mechanistic insight of this study is the identification of IGF2BP3 as the functional mediator of LINC01671-driven metabolic regulation. IGF2BP3 is a well-characterized RNA-binding protein and m^6A “reader” that stabilizes oncogenic transcripts through recognition of specific RNA motifs and epitranscriptomic modifications[37]. Accumulating evidence establishes IGF2BP3 as a pivotal m^6A reader in tumor progression. Prior studies have shown that IGF2BP3 stabilizes oncogenic ECT2 transcripts downstream of RBM15, thereby driving epithelial–mesenchymal transition and modulating chemotherapy response[38]. Another study demonstrates that IGF2BP3 cooperates with METTL3 and ILF3 to stabilize PCSK9 mRNA, promoting hepatocellular carcinoma progression[39]. In triple-negative breast cancer, IGF2BP3 further sustains cancer stemness and carboplatin resistance by maintaining FZD1/7 mRNA stability and activating β-catenin signaling, reinforcing its role as an epitranscriptomic driver and therapeutic vulnerability[40]. Our study demonstrates that LINC01671 physically associates with IGF2BP3, thereby enhancing LINC01671 stability and promoting LDHA expression, ultimately sustaining a pro-glycolytic program. These findings support a feed-forward regulatory circuit in which lncRNA–RBP interactions reinforce the expression of key metabolic enzymes.

From a translational perspective, our findings highlight a dual opportunity for clinical intervention. First, LINC01671 expression serves as a robust biomarker for glycolytic dependency, potentially identifying patients most likely to respond to metabolic therapies. Second, while direct LDHA inhibitors are currently under investigation, targeting the upstream LINC01671-mediated regulation offers a strategy with superior tumor specificity. Given the emerging feasibility of RNA-based therapeutic platforms across a broad of diseases[41], disrupting this lncRNA-dependent metabolic shield represents a promising therapeutic avenue to sensitize OCCC to conventional platinum-based treatments. RNA-based therapeutics offer distinct advantages, notably the capacity to target genetic determinants previously considered “undruggable” by conventional small molecules or antibodies, and are demonstrating broad translational potential across diverse diseases[42]. In oncology, RNA-directed strategies enable precise modulation of oncogenic drivers and signaling pathways, thereby facilitating molecularly tailored interventions[43]. Among these approaches, antisense oligonucleotides (ASOs) exert therapeutic effects by selectively binding target pre-mRNAs or mRNAs, promoting transcript degradation or interfering with RNA processing[44]. Emerging clinical evidence indicates that ASO-based therapies, administered either as monotherapy or in combination with immunotherapy, can confer clinical benefit in patients with advanced malignancies[45]. Moreover, advances in nanoparticle-based delivery systems have

substantially improved the efficacy and tolerability of ASO therapeutics, accelerating their clinical translation[46].

More broadly, lncRNAs frequently orchestrate metabolic programs by serving as molecular scaffolds for RNA-binding proteins[47]. Our data establish IGF2BP3—an oncofetal RBP with established roles in tumor progression—as an indispensable partner of LINC01671 in OCCC. lncRNAs adopt defined structural domains that are intimately linked to their function, making them attractive and viable targets for therapeutic intervention[48]. Targeting such RNA–protein complexes represents a conceptual shift from conventional enzyme inhibition toward disruption of upstream regulatory scaffolds. Small molecules or RNA-based therapeutics designed to interfere with IGF2BP3–RNA interactions may attenuate LDHA-driven glycolysis at its regulatory source while potentially improving therapeutic specificity.

Several limitations merit consideration. Although our in vitro and xenograft data support a central role for the IGF2BP3/LINC01671/LDHA axis in driving glycolysis and tumor growth, metabolic flux analyses in patient-derived models would further strengthen the translational relevance of these findings. In addition, while transcriptomic analyses indicated that LINC01671 is primarily involved in glycolytic pathways and antigen processing and presentation, while our data clearly implicate the LINC01671/LDHA axis in T-cell suppression, future studies employing single-cell RNA sequencing and extracellular flux analysis (Seahorse) in immunocompetent models will be instrumental in dissecting the dynamic crosstalk between glycolytic byproducts and specific immune cell subsets. Mechanistically, while we confirmed cytoplasmic co-localization and physical interaction among LINC01671, IGF2BP3 and LDHA mRNA, the precise structural elements of LINC01671 responsible for binding the KH domains of IGF2BP3 and LDHA remain to be defined. Mapping these interaction motifs would refine our understanding of the specificity and stability of this regulatory complex. Given the molecular heterogeneity of OCCC, validation in larger, clinically annotated cohorts is also required to determine whether LINC01671 expression correlates with glycolytic dependency, therapeutic response, or clinical outcome.

Conclusions

In summary, our study identifies the IGF2BP3/LINC01671/LDHA axis as a critical metabolic driver of OCCC (Fig. 9). By linking lncRNA–RBP interactions to sustained glycolysis and malignant progression, these findings provide mechanistic insight into OCCC biology and suggest new avenues for metabolism-directed therapeutic intervention.

Declarations

Ethics approval and consent to participate

This study was conducted in accordance with the Declaration of Helsinki. Ethical approval was granted by the Ethics Committee of Fudan University Shanghai Cancer Center under Approval No. 050432-4-

2108* dated 10 August 2021. Written informed consent was obtained from all human participants prior to inclusion in the research.

Consent for publication

Informed consent was obtained from all the authors of this study.

Competing interests

The authors have no relevant financial or non-financial interests to disclose.

Funding

This work was supported by grants from the National Natural Foundation Science of China (NSFC 81802597) and the National Natural Foundation Science of China (NSFC 82303274).

Author Contribution

Xiaonan Zhou: Conceptualization, Formal analysis, Investigation, Methodology, Validation, Visualization, Writing – original draft.Yifei Liu: Data curation, Formal analysis, Investigation, Validation, Writing – original draftJing Gao: Data curation, Formal analysis, Investigation, Methodology.Ling Cui: Data curation, Formal analysis, Investigation, Resources.Hui Li: Data curation, Funding acquisition, Investigation, Resources.Huijuan Ge: Investigation, Resources, Visualization.Lin Yu: Formal analysis, Investigation, Resources, Supervision.Jiaojie Lv: Investigation, Software, Supervision, Validation.Ke Zuo: Data curation, Investigation, Software, Visualization.Tian Tian: Formal analysis, Investigation, Methodology, Resources, Supervision.Yue Wang: Data curation, Investigation, Methodology, Software, Visualization.Hui Sun: Data curation, Investigation, Methodology, Software, Visualization.Yufan Cheng: Formal analysis, Investigation, Methodology, Resources, Supervision.Rui Bi: Conceptualization, Funding acquisition, Methodology, Project administration, Supervision, Validation, Writing – review and editing.

Acknowledgements

Not applicable.

Data Availability

All data supporting the findings of this study are available within the paper and its Supplementary Information.

References

1. 1. Bray F, Laversanne M, Sung H, Ferlay J, Siegel RL, Soerjomataram I, Jemal A: **Global cancer statistics 2022: GLOBOCAN estimates of incidence and mortality worldwide for 36 cancers in 185 countries**. *CA Cancer J Clin* 2024, **74**(3):229–263.
2. 2. Machida H, Matsuo K, Yamagami W, Ebina Y, Kobayashi Y, Tabata T, Kanauchi M, Nagase S, Enomoto T, Mikami M: **Trends and characteristics of epithelial ovarian cancer in Japan between 2002 and 2015: A JSGO-JSOG joint study**. *Gynecol Oncol* 2019, **153**(3):589–596.
3. 3. Passarelli A, Cecere SC, Ventriglia J, Pisano C, De Cecio R, Rossetti S, Tambaro R, Di Napoli M, Lobianco L, Calvanese G *et al*: **The immunotherapy era in ovarian clear cell carcinoma: current evidence and future perspective**. *Front Immunol* 2025, **16**:1661048.
4. 4. Nie H, Liao L, Zielinski RJ, Gomez JA, Basi AV, Seeley EH, Tan L, Bilecz AJ, Zhou W, Liu H *et al*: **Selective Alanine Transporter Utilization Is a Therapeutic Vulnerability in ARID1A-Mutant Ovarian Cancer**. *Cancer Res* 2025, **85**(18):3471–3489.
5. 5. Jiang M, Yamaguchi K, Hamada K, Hosoe Y, Mise Y, Kitamura S, Liu Z, Wei H, Gao Z, Taki M *et al*: **HIF2A as a prognostic and clinical therapeutic target in ovarian clear cell carcinoma**. *Int J Cancer* 2026.
6. 6. Tylichova Z, Krkoska M, Hrabal V, Stenckova M, Vojtesek B, Coates PJ: **Heterogeneity of glucose metabolism and uptake identifies distinct cancer cell and cancer stem cell phenotypes**. *Cell Mol Biol Lett* 2026, **31**(1):8.
7. 7. Li X, Qin X, Zhao X, Liu Y, Wang L, Li K, Li J, Ma J, Dai L, Hasim A: **Spatial multi-omics guides ASCT2-targeted delivery of glycolysis inhibitor for cervical cancer suppression and chemoresistance reversal**. *J Adv Res* 2025.
8. 8. Zhang W, Xia M, Li J, Liu G, Sun Y, Chen X, Zhong J: **Warburg effect and lactylation in cancer: mechanisms for chemoresistance**. *Mol Med* 2025, **31**(1):146.
9. 9. Chen Y, Qian Y, Shi J, Wang Y, Fu T, Meng S, Wang M, Fu M, Zhang J, Zhang X *et al*: **LINC00973/DTX3L Axis Promotes Non-Small Cell Lung Cancer Progression and Serves as a Therapeutic Target**. *Smart Med* 2026, **5**(1):e70029.
10. 10. Hsu KW, Chang JS, Lai JC, Yang LH, Peng PH, Lin TC, Wu KJ: **Scaffolding of the H4K5ac chromatin remodeling complex by lncRNA MAHAC mediates epithelial-mesenchymal transition**. *Nucleic Acids Res* 2026, **54**(4).
11. 11. Ren L, Fang X, Shrestha SM, Ji Q, Ye H, Liang Y, Liu Y, Feng Y, Dong J, Shi R: **LncRNA SNHG16 promotes development of oesophageal squamous cell carcinoma by interacting with EIF4A3 and modulating RhoU mRNA stability**. *Cell Mol Biol Lett* 2022, **27**(1):89.
12. 12. Sharma H, Valentine MNZ, Toki N, Sueki HN, Gustincich S, Takahashi H, Carninci P: **Decryption of sequence, structure, and functional features of SINE repeat elements in SINEUP non-coding RNA-mediated post-transcriptional gene regulation**. *Nat Commun* 2024, **15**(1):1400.

13. 13. Hochberg-Laufer H, Schwed-Gross A, Neugebauer KM, Shav-Tal Y: **Uncoupling of nucleo-cytoplasmic RNA export and localization during stress**. *Nucleic Acids Res* 2019, **47**(9):4778–4797.
14. 14. Kilgas S, Syed A, Toolan-Kerr P, Swift ML, Roychoudhury S, Sarkar A, Wilkins S, Quigley M, Poetsch AR, Botuyan MV *et al*: **NEAT1 modulates the TIRR/53BP1 complex to maintain genome integrity**. *Nat Commun* 2024, **15**(1):8438.
15. 15. P LY, Pan H, Hu K, Xue Y, Li Q, Lin R, Zheng S, Guo Z, Guo K: **The LEPIS-HuR-TMOD4 axis regulates hepatic cholesterol homeostasis and accelerates atherosclerosis**. *Atherosclerosis* 2024, **393**:117554.
16. 16. Yang L, Guo G, Yu X, Wen Y, Lin Y, Zhang R, Zhao D, Huang Z, Wang G, Yan Y *et al*: **Mutation-Derived Long Noncoding RNA Signature Predicts Survival in Lung Adenocarcinoma**. *Front Oncol* 2022, **12**:780631.
17. 17. Geng W, Lv Z, Fan J, Xu J, Mao K, Yin Z, Qing W, Jin Y: **Identification of the Prognostic Significance of Somatic Mutation-Derived LncRNA Signatures of Genomic Instability in Lung Adenocarcinoma**. *Front Cell Dev Biol* 2021, **9**:657667.
18. 18. Yin W, Wang JH, Liang YM, Liu KH, Chen Y, Chen YS: **Effects of Purine Metabolism-Related LINC01671 on Tumor Heterogeneity in Kidney Renal Clear Cell Carcinoma**. *Front Biosci (Landmark Ed)* 2023, **28**(12):354.
19. 19. Huang RY, Lin JJ: **Ovarian Clear Cell Carcinoma: An Endometriosis-Associated Cancer with Therapeutic Challenges**. *Cold Spring Harb Perspect Med* 2025, **15**(8).
20. 20. Chen J, Huang Z, Chen Y, Tian H, Chai P, Shen Y, Yao Y, Xu S, Ge S, Jia R: **Lactate and lactylation in cancer**. *Signal Transduct Target Ther* 2025, **10**(1):38.
21. 21. Dong Z, Yuan Z, Jin T, Gao C, Wang X, Xu F: **Lactate at the crossroads of tumor metabolism and immune escape: a new frontier in cancer therapy**. *J Transl Med* 2025, **23**(1):1239.
22. 22. Zhong X, Wang Y, He X, He X, Hu Z, Huang H, Chen J, Chen K, Wei P, Zhao S *et al*: **HIF1A-AS2 promotes the metabolic reprogramming and progression of colorectal cancer via miR-141-3p/FOXC1 axis**. *Cell Death Dis* 2024, **15**(9):645.
23. 23. Yi T, He J, Pan M, Wang Y, Lin C, Ye Y, Yang W, Ye X, Ning D, Lan J *et al*: **LL22NC03-N14H11.1 regulates the m6A modification of MYC and promotes glycolytic activity in hepatocellular carcinoma cells by inhibiting IGF2BP3 ubiquitination degradation**. *J Exp Clin Cancer Res* 2025, **45**(1):14.
24. 24. Xue ZR, Xin YY, Jin WL: **Exploiting metabolic vulnerabilities in cancer: From mechanisms to therapeutic opportunities**. *Cancer Lett* 2025, **634**:218067.
25. 25. Zhu Y, Yan W, Tong L, Yang J, Ge S, Fan J, Jia R, Wen X: **Metabolic Reprogramming: A Crucial Contributor to Anticancer Drug Resistance**. *MedComm (2020)* 2025, **6**(9):e70358.
26. 26. Rosso R, Turinetto M, Borella F, Chopin N, Meeus P, Laine A, Ray-Coquard I, Le Saux O, Ferraioli D: **Ovarian clear cell carcinoma: open questions on the management and treatment algorithm**. *Oncologist* 2025, **30**(1).

27. 27. Khan F, Lin Y, Ali H, Pang L, Dunterman M, Hsu WH, Frenis K, Grant Rowe R, Wainwright DA, McCortney K *et al*: **Lactate dehydrogenase A regulates tumor-macrophage symbiosis to promote glioblastoma progression**. *Nat Commun* 2024, **15**(1):1987.
28. 28. Zhang Y, Wang J, Li C, Lei Z, Zhao X, Xuan X, Sukocheva O, Tse E, Liu J: **Protein lactylation in cancer and other pathologies: Epigenetic regulation of glycolysis and its therapeutic perspectives**. *Semin Cancer Biol* 2026, **118**:28–43.
29. 29. Xie F, Zhang H, Dai X, Tu M, Yu C, Liu L, Guo Y, Sun H, Gao Q, Wang J *et al*: **HPD is an RNA-Binding Protein Sustaining Ovarian Cancer Cell Glycolysis, Tumor Growth, and Drug Resistance**. *Adv Sci (Weinh)* 2025, **12**(30):e03999.
30. 30. Lin TY, Gu SY, Lin YH, Shih JH, Lin JH, Chou TY, Lee YC, Chang SF, Lang YD: **Paclitaxel-resistance facilitates glycolytic metabolism via Hexokinase-2-regulated ABC and SLC transporter genes in ovarian clear cell carcinoma**. *Biomed Pharmacother* 2024, **180**:117452.
31. 31. Erdem A, Kaye S, Caligiore F, Johanns M, Leguay F, Schuringa JJ, Ito K, Bommer G, van Gastel N: **Lactate dehydrogenase A-coupled NAD(+) regeneration is critical for acute myeloid leukemia cell survival**. *Cancer Metab* 2025, **13**(1):22.
32. 32. Yuan Y, Xiao Y, Zou J, Luo L, Li M, Shen K, Wei L, Zhang Y, Wang P, Chen Y *et al*: **Lactate derived from macrophages drives skin dermal fibroblasts phenotypic remodeling via MCT1-primed histone H3 lysine 23 lactylation in hypertrophic scar**. *Nat Commun* 2026.
33. 33. Ding Y, Tian Y, Ren W, Hu X, Li M, Liu B, Chen C, Lu Y, Li L, Yan W *et al*: **SLC2A3-Mediated Lactate Metabolism Promotes Lung Cancer Bone Metastasis by Modulating P53 Lactylation and Immune Evasion**. *Adv Sci (Weinh)* 2026:e16622.
34. 34. Zhang D, Tang Z, Huang H, Zhou G, Cui C, Weng Y, Liu W, Kim S, Lee S, Perez-Neut M *et al*: **Metabolic regulation of gene expression by histone lactylation**. *Nature* 2019, **574**(7779):575–580.
35. 35. Yang Y, Wu Y, Guo X, Gan WJ, Wu WX, Shi WY, He XS, Liu YX, Wan S, Jiang Z *et al*: **Extracellular CD44 lactylation impairs CD8(+) T cell function in KRAS-mutant colorectal cancer**. *Nat Metab* 2026.
36. 36. Chen H, Li Y, Li H, Chen X, Fu H, Mao D, Chen W, Lan L, Wang C, Hu K *et al*: **NBS1 lactylation is required for efficient DNA repair and chemotherapy resistance**. *Nature* 2024, **631**(8021):663–669.
37. 37. Zhu TY, Hong LL, Ling ZQ: **Oncofetal protein IGF2BPs in human cancer: functions, mechanisms and therapeutic potential**. *Biomark Res* 2023, **11**(1):62.
38. 38. Zhu X, Chen H, Xu K, Liu Y, Li H, Sang Y, Zhao Y, Liu X, Wang X, Cui X *et al*: **RBM15 Enhances 5-Fluorouracil Drug Sensitivity and Suppresses Gastric Cancer Progression by Modulating N6-Methyladenosine Modification of ECT2-Dependent IGF2BP3**. *Research (Wash D C)* 2026, **9**:1108.
39. 39. Wang WL, Yen CC, Yen CS, Huang YH, Huang HY, Chen JF, Liu YY, Wang ST, Liu YT, Hung MC *et al*: **Dysregulation of PCSK9 via m(6)A-dependent epitranscriptomic programs fosters hepatocellular carcinoma progression**. *Cancer Lett* 2026, **640**:218255.
40. 40. Cai MY, Yin P, Wang ZW, Huang YZ, Wang YX, Wu KF, Zhang X, Shi L, Wei JF, Ding Q: **Dual regulation of FZD1/7 by IGF2BP3 enhances stem-like properties and carboplatin resistance in triple-negative breast cancer**. *Cancer Lett* 2025, **632**:217944.

41. 41. Navid Talemi M, Ramezani Farani M, Alipour Eskandani N, Mirzaee D, Alipourfard I, Huh YS: **Programmable lipid nanoparticles for RNA therapeutics: Design principles and clinical translation**. *Mater Today Bio* 2026, **37**:102774.
42. 42. Torrisi SA, Geraci F, Diolosa L, De Luca A, Falzone L, Drago F, Libra M, Leggio GM: **RNA-based drugs: current, imminent and possible therapeutic applications**. *Pharmacol Ther* 2026, **277**:108958.
43. 43. Sarker D, Plummer R, Meyer T, Sodergren MH, Basu B, Chee CE, Huang KW, Palmer DH, Ma YT, Evans TRJ *et al*: **MTL-CEBPA, a Small Activating RNA Therapeutic Upregulating C/EBP-alpha, in Patients with Advanced Liver Cancer: A First-in-Human, Multicenter, Open-Label, Phase I Trial**. *Clin Cancer Res* 2020, **26**(15):3936–3946.
44. 44. Zhao Y, Yang G, Zhang Z, Xie M, Liu J, Cheng Y, Zhang Y, Zhang X, Wang Y, Ma D *et al*: **Targeting coronaviral inflammation: aptamer-based strategies for emerging threats**. *Signal Transduct Target Ther* 2026, **11**(1):54.
45. 45. Siu LL, Postel-Vinay S, Villanueva-Vazquez R, de Velasco G, Castanon Alvarez E, Kyriakopoulos CE, Johnson M, Ouali K, McMorn S, Angell HK *et al*: **AZD8701, an Antisense Oligonucleotide Targeting FOXP3 mRNA, as Monotherapy and in Combination with Durvalumab: A Phase I Trial in Patients with Advanced Solid Tumors**. *Clin Cancer Res* 2025, **31**(8):1449–1462.
46. 46. Ou YH, Chng WH, Muthuramalingam RPK, Raghunathan P, Khunkitchai N, Lee CK, Jun JH, Ng ZX, Xin PT, Goh WJ *et al*: **Delivery of Antisense Oligonucleotides Using the Nano-Cell Vesicle Technology System (nCVTs) for Targeted Cancer Therapy**. *Small* 2026, **22**(8):e09094.
47. 47. Shen T, Wang H, Tang B, Zhu G, Wang X: **The impact of RNA binding proteins and the associated long non-coding RNAs in the TCA cycle on cancer pathogenesis**. *RNA Biol* 2023, **20**(1):223–234.
48. 48. Watmuff H, Crawford A, Eusse B, Jones AN: **Structure-function-guided drug development efforts to target lncRNAs**. *Trends Pharmacol Sci* 2025, **46**(8):703–721.

Figures

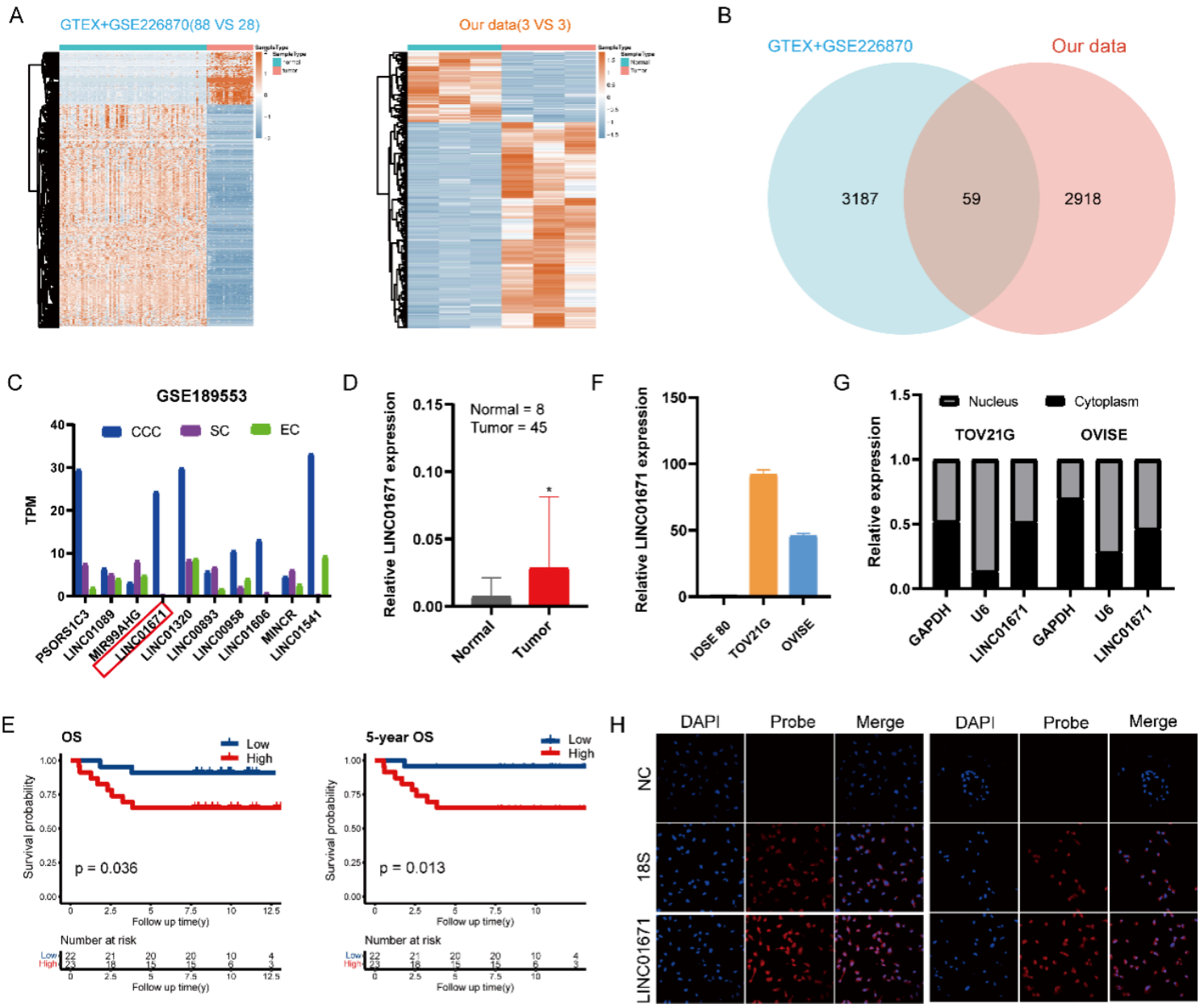


Figure 1

Identification of LINC01671 as a lncRNA associated with the poor prognosis of OCCC.

A Heatmaps show some differentially-expressed lncRNAs in the GSE226870 dataset (left) and the FUSCC-OCCC dataset (right).

B Veen plot show differentially expressed lncRNAs, which exist in both datasets.

C Lineage-specific expression of LINC01671 in GSE189553 dataset.

D Relative LINC01671 expression in OCCC tissues and normal tissues.

E Kaplan–Meier curve comparing the OS and 5-year OS between the LINC01671-high group and LINC01671-low group in the FUSCC cohort.

F Relative LINC01671 expression in OCCC cell lines.

G Relative LINC01671 expression in subcellular fractions.

H FISH images showing the subcellular distribution of LINC01671 in TOV21G (left) and OVISE cells (right).

*P<0.05; **P <0.01; ***P<0.001; ns no significance.

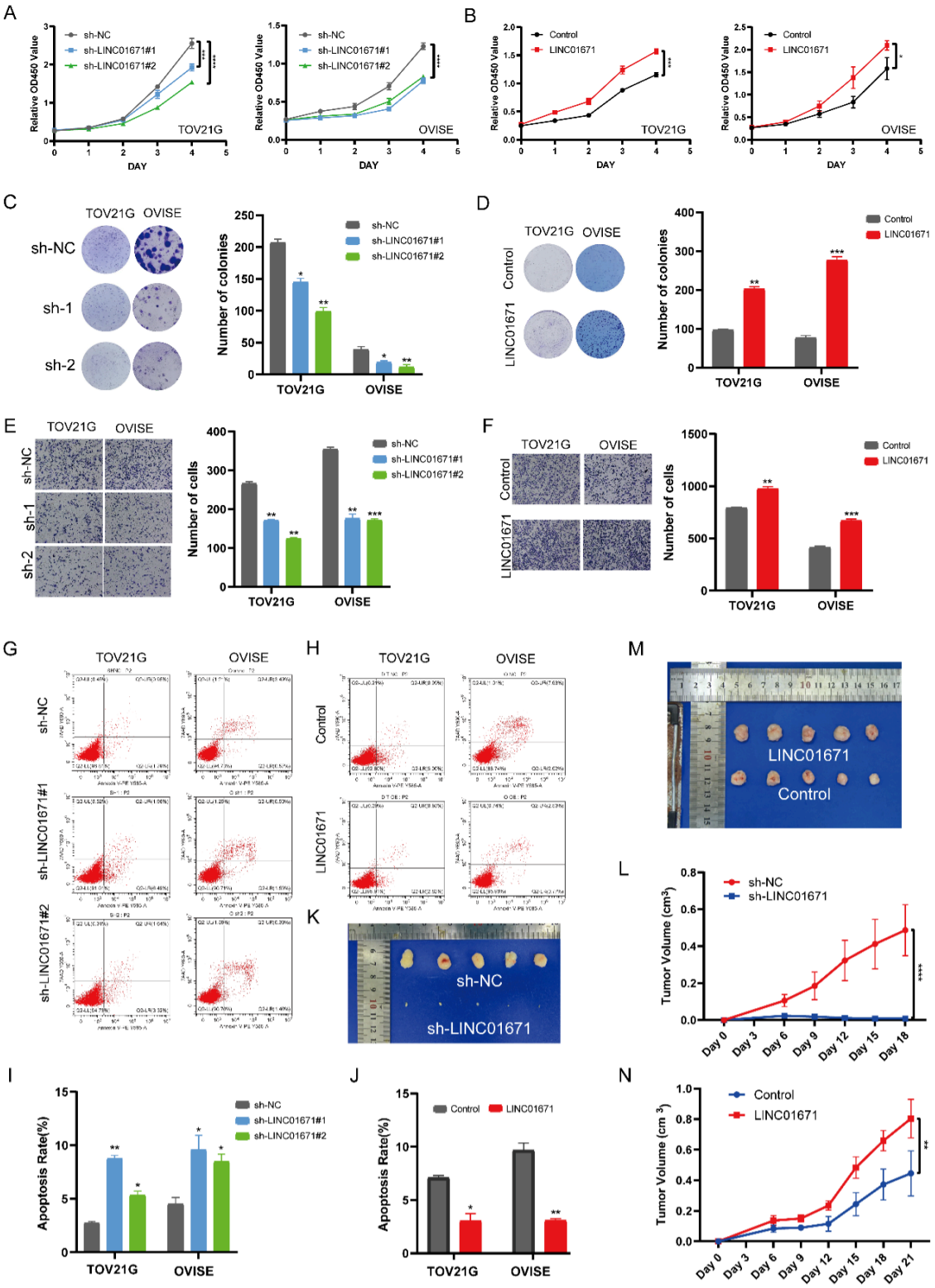


Figure 2

LINC01671 promotes malignant phenotypes of OCCC cells in vitro and in vivo.

A,B The viabilities of TOV21G and OVISE cells after overexpressing or silencing LINC01671.

C,D Colony formation assay of TOV21G and OVISE cells after overexpressing or silencing LINC01671.

E,F Transwell invasion assay of TOV21G and OVISE cells after overexpressing or silencing LINC01671.

G-J Flow cytometric analysis of apoptosis showing increased apoptosis following LINC01671

knockdown and decreased apoptosis upon LINC01671 overexpression.

K,L Representative images and Growth curve of subcutaneous xenograft tumors demonstrating suppressed tumor growth upon LINC01671 knockdown in vivo.

M,N Enhanced tumor growth in xenograft models derived from LINC01671-overexpressing cells. *P<0.05; **P <0.01; ***P<0.001; ns no significance.

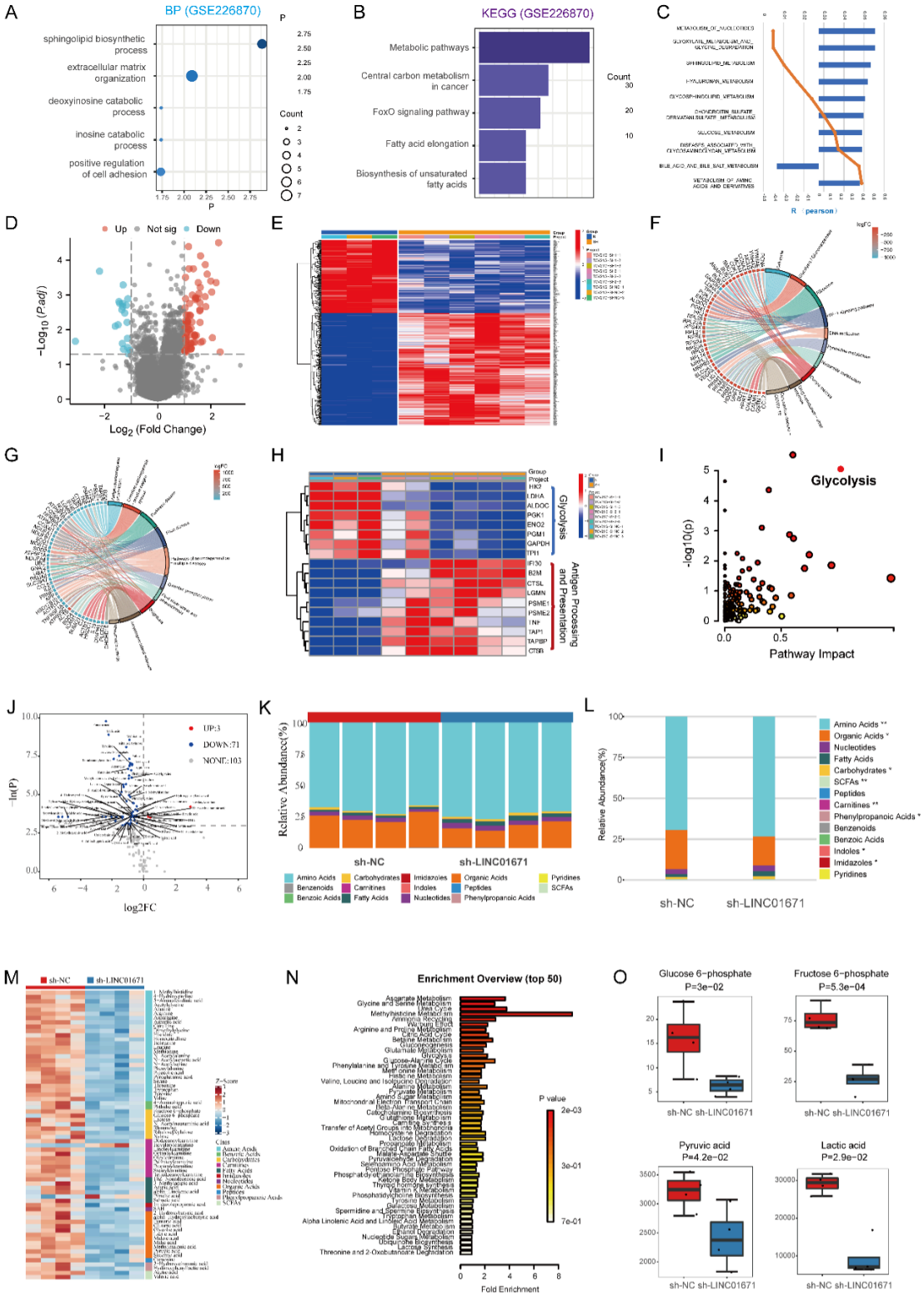


Figure 3

LINC01671 regulates aerobic glycolysis in OCCC.

A-C, Functional characterization of LINC01671-correlated genes in the GSE226870 dataset ($r > 0.5$, $P < 0.05$). A, Gene Ontology (GO) network of biological processes associated with the top 200 correlated genes positively correlated with LINC01671 expression in the GSE226870 dataset. B, KEGG pathway

enrichment analysis highlighting central carbon metabolism. C, Gene set variation analysis (GSVA) based on the Reactome database showing LINC01671-associated metabolic alterations.

D–H, Transcriptomic profiling of TOV21G cells upon LINC01671 knockdown. D, Volcano plot of differentially expressed genes (DEGs; |log_2FC| > 1, P < 0.05). E, Heatmap showing the top DEGs between sh-NC (n = 3) and sh-LINC01671 (n = 6) groups. KEGG enrichment analysis of significantly downregulated (F) and upregulated (G) genes. H, Heatmaps illustrating expression shifts in glycolytic and antigen-processing genes.

I, Pathway impact analysis using MetaboAnalyst identifying glycolysis as a major downstream pathway regulated by LINC01671.

J–O, Comprehensive targeted metabolomic profiling (Q300) of TOV21G cells. J, Overview of significantly altered metabolites detected by targeted metabolomics following LINC01671 knockdown. K, L, Category-specific metabolic shifts and representative metabolite distributions. M, N, Heatmap and enrichment analysis of significantly altered metabolites highlighting the Warburg effect pathway. O, Relative abundance of key glycolytic intermediates, including glucose-6-phosphate (G6P), fructose-6-phosphate (F6P), pyruvate, and lactate. Data in O are presented as mean ± s.d.

*P<0.05; **P <0.01; ***P<0.001; ns no significance.

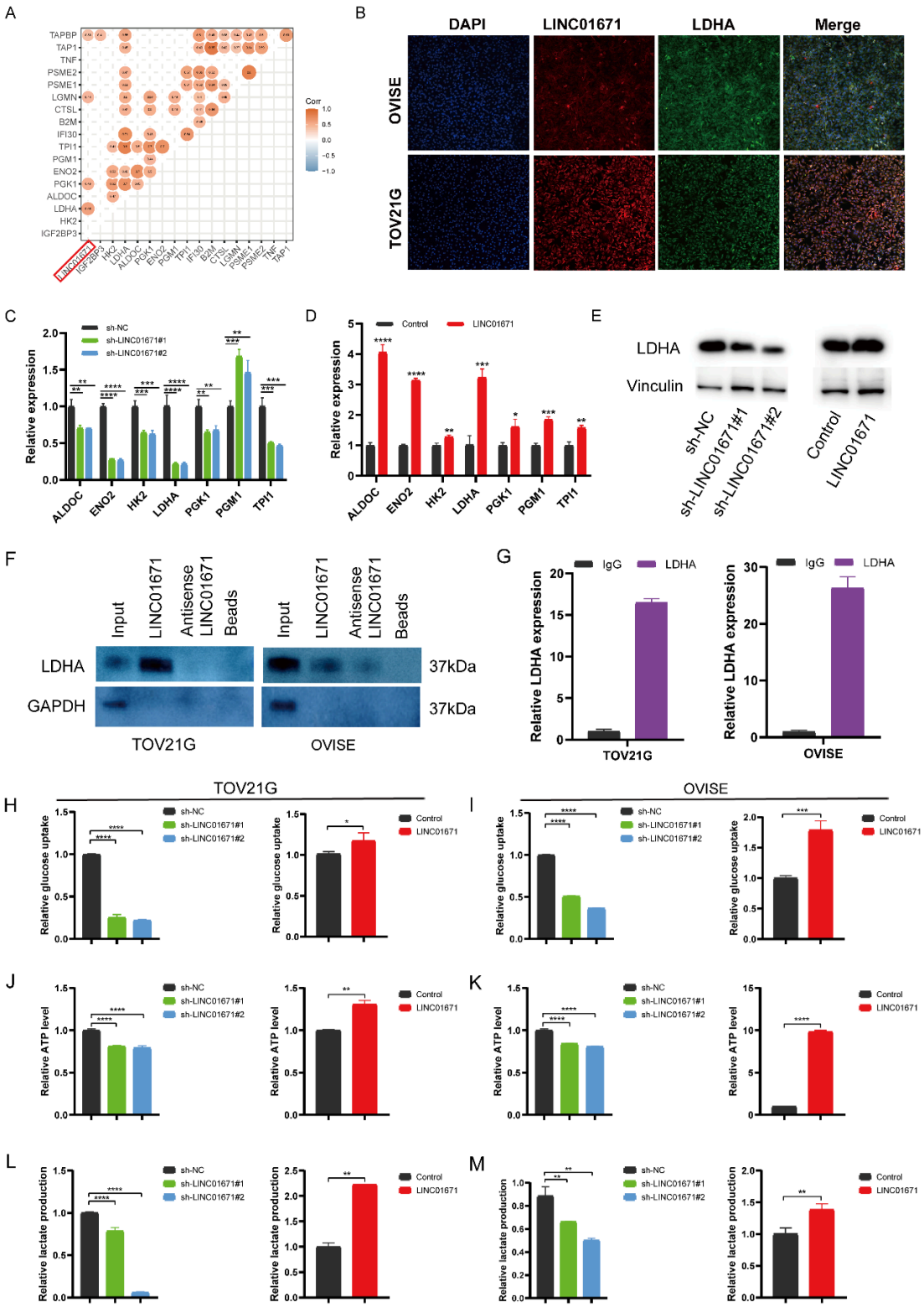


Figure 4

LINC01671 promotes glycolysis by interacting with and regulating LDHA.

A Correlation analysis between LINC01671 and glycolytic gene expression levels based on transcriptome sequencing data (GSE226870, r = 0.58).

B Representative co-immunostaining images showing the spatial colocalization of LINC01671 (red) and LDHA (green) in OCCC cells.

C,D RT–qPCR analysis of glycolysis-related gene expression following LINC01671 knockdown (C) or overexpression (D) in TOV21G and OVISE cells.

E The protein levels of LDHA of OCCC cells after overexpressing or silencing LINC01671.

F Western blotting of proteins obtained by RNA pull-down assay showed that LINC01671 bound to LDHA.

G RIP assays confirmed that LINC01671 interacts with LDHA.

H-M, Glucose uptake (H,I), ATP production (J,K), and lactate production (L,M) assays in TOV21G and OVISE cells following LINC01671 knockdown or overexpression.

*P<0.05; **P<0.01; ***P<0.001; ns no significance.

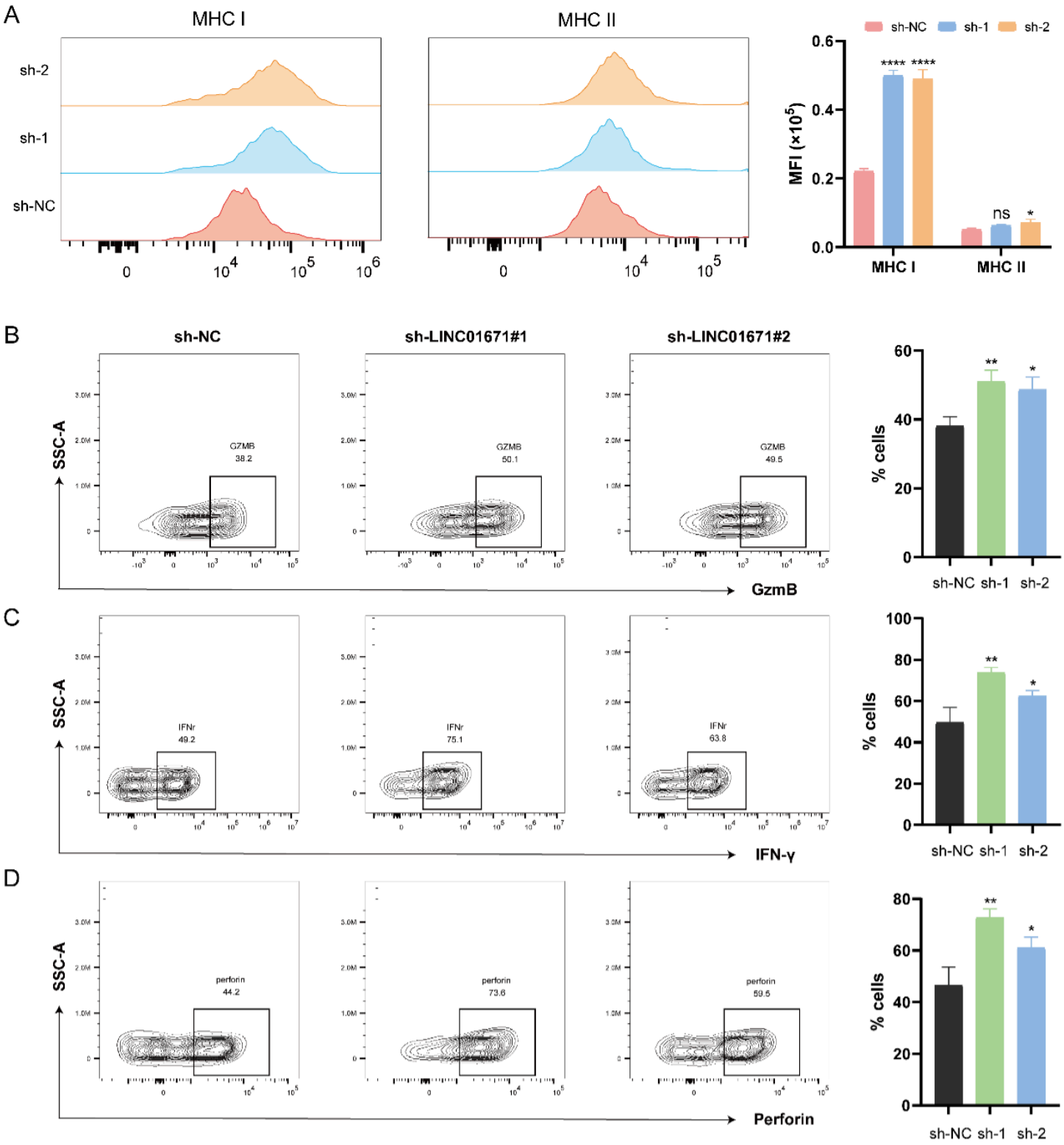


Figure 5

LINC01671 modulates tumor antigen presentation and impairs CD8+ T cell effector function in TOV21G cell.

A. Flow cytometric analysis of MHC I and II expression on tumor cells.

B-D. Flow cytometry-based T cell cytotoxic assay. The experimental cohorts were cocultured with CD8+T cells. Intracellular GzmB (B), IFN-γ (C) and perforin (D) expression analysis after cell membrane permeabilization.

*P<0.05; **P<0.01; ***P<0.001; ns no significance.

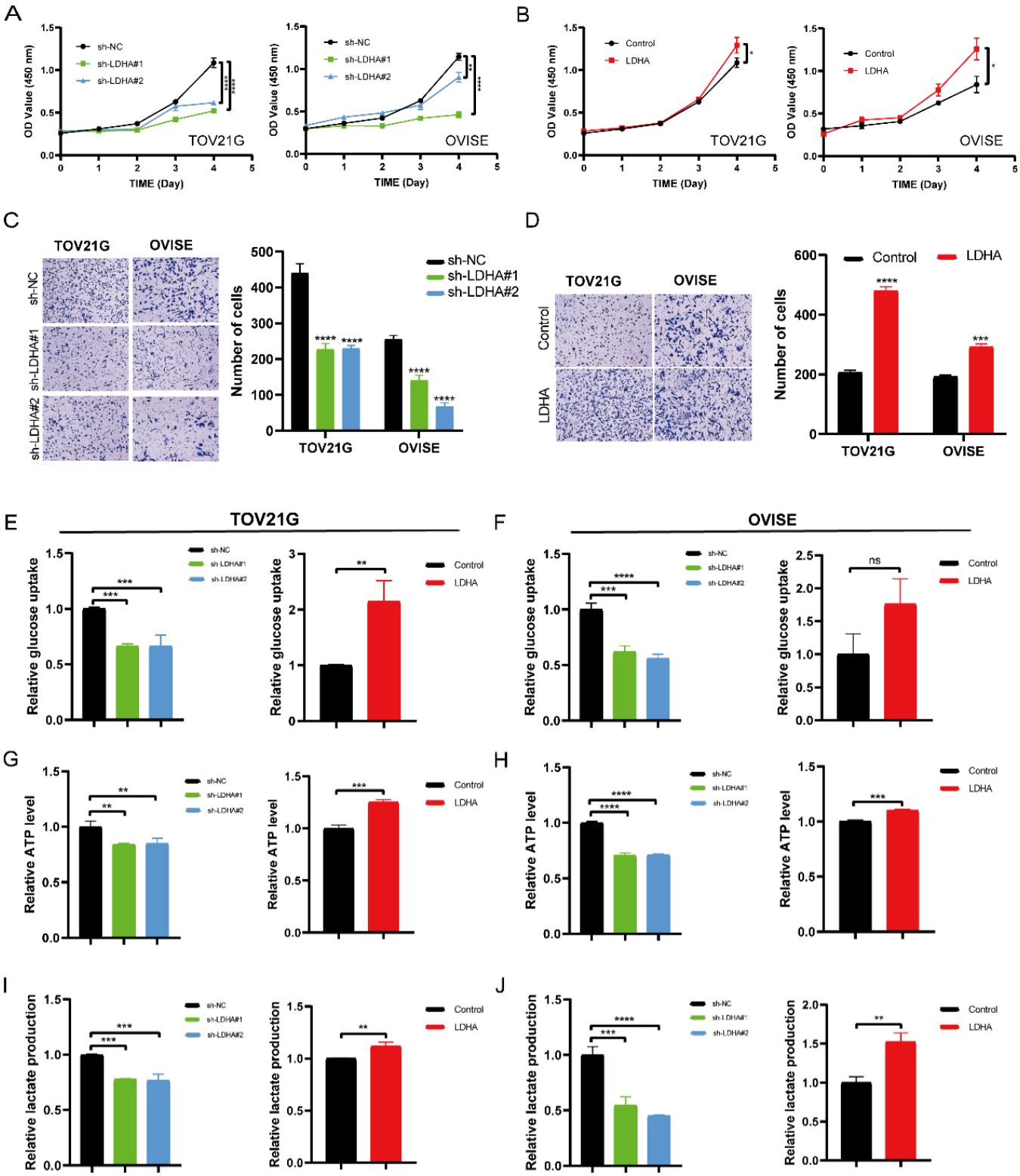


Figure 6

LDHA promotes proliferation, invasion and aerobic glycolysis in OCCC cells.

A,B The viabilities of TOV21G and OVISE cells after overexpressing or silencing LDHA.

C,D Transwell invasion assay of TOV21G and OVISE cells after overexpressing or silencing LDHA. E-J, Glucose uptake (E,F), ATP production (G,H), and lactate production (I,J) assays in TOV21G and OVISE cells following LINC01671 knockdown or overexpression.

*P<0.05; **P<0.01; ***P<0.001; ns no significance.

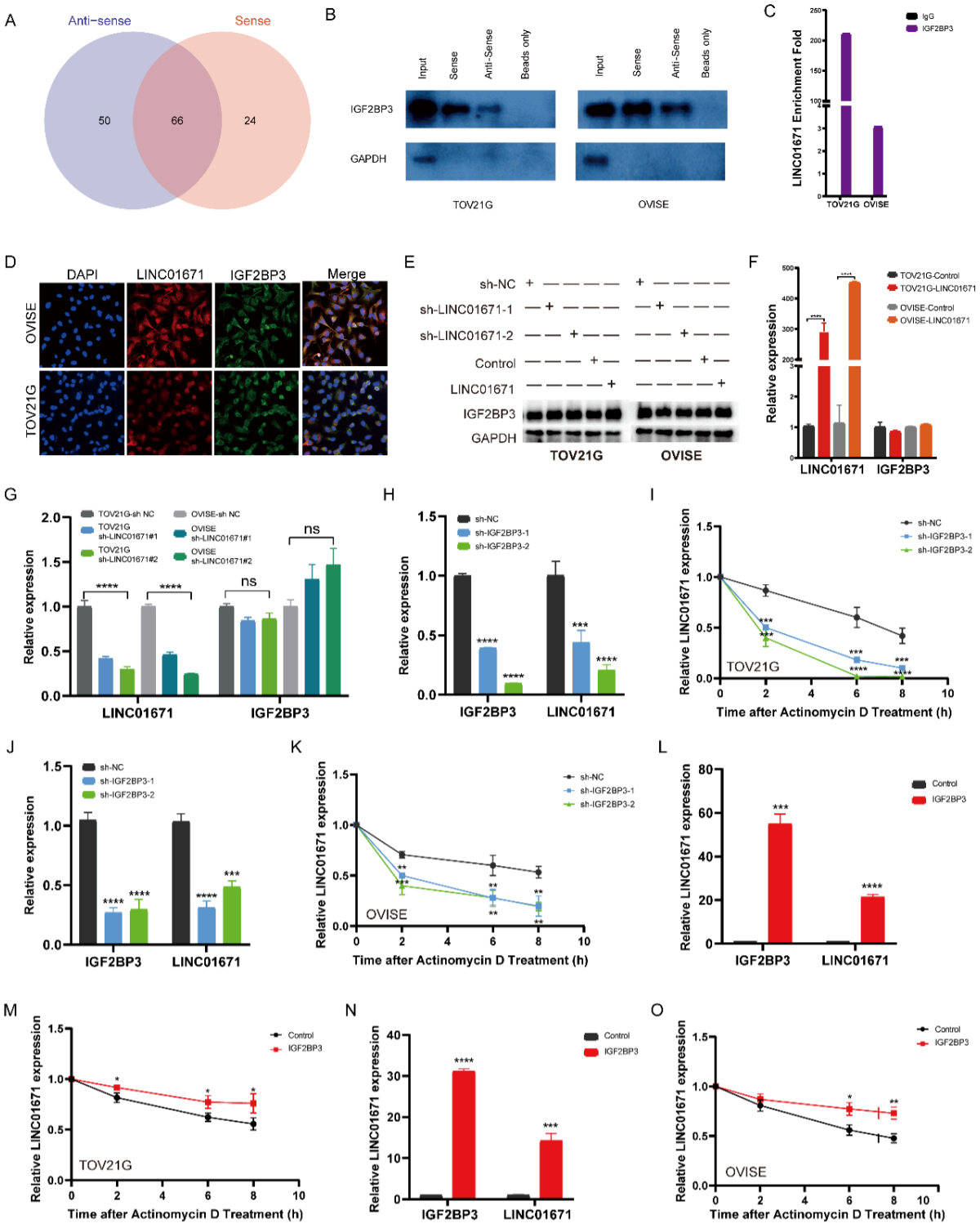


Figure 7

IGF2BP3 interacts with and stabilizes LINC01671 in OCCC cells.

A Venn diagram showing proteins enriched by biotinylated LINC01671 sense and antisense probes following RNA pull-down.

B Western blotting of proteins obtained by RNA pull-down assay showed that LINC01671 bound to IGF2BP3.

C RIP assays confirmed that LINC01671 interacts with IGF2BP3.

D FISH and IF assays show LINC01671 (red) and IGF2BP3 (green) are co-localized in the cytoplasm in OCCC cells.

E-G Western blot and RT–qPCR analyses showing that LINC01671 knockdown or overexpression does not alter IGF2BP3 RNA or protein levels in TOV21G and OVISE cells.

H-O Effects of IGF2BP3 silencing or overexpression on LINC01671 RNA abundance and transcript stability, assessed by RT–qPCR and mRNA stability assays in OCCC cells.

*P<0.05; **P<0.01; ***P<0.001; ns no significance.

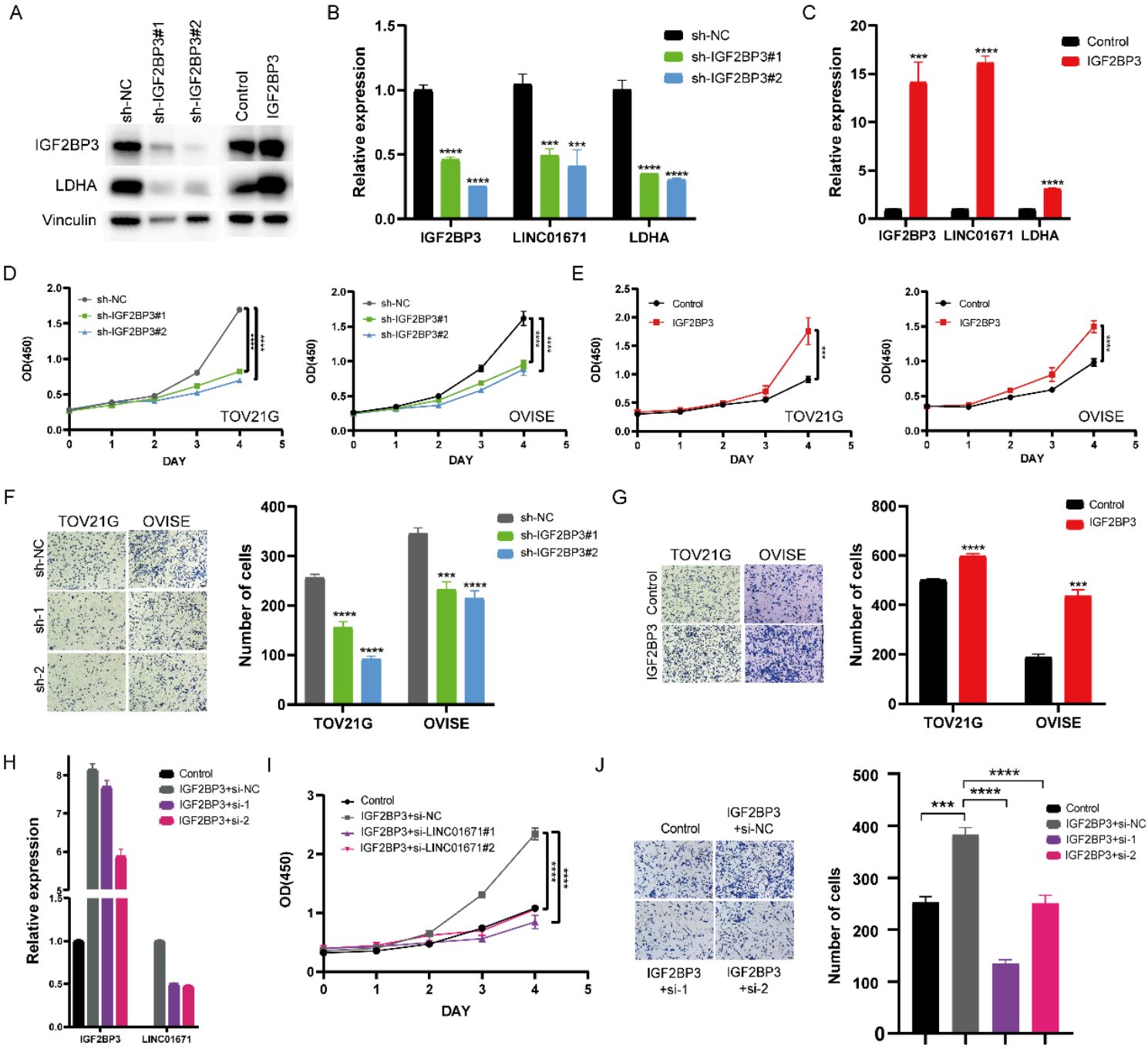


Figure 8

IGF2BP3/LINC01671/LDHA axis regulates OCCC progression

A LDHA protein levels were analyzed by western blot following IGF2BP3 knockdown or overexpression.

B,C IGF2BP3, LINC01671 and LDHA mRNA levels were quantified by RT-qPCR following IGF2BP3 knockdown or overexpression.

D,E The viabilities of TOV21G and OVISE cells after overexpressing or silencing IGF2BP3.

F,G Transwell invasion assay of TOV21G and OVISE cells after overexpressing or silencing IGF2BP3.

H RT-qPCR analysis showing the RNA level of IGF2BP3 and LINC01671 in OCCC cells with different treatments.

I,J Rescue assays showing that silencing of LINC01671 significantly attenuated the IGF2BP3 overexpression–mediated increase in cell proliferation (i) and invasion (j).

*P<0.05; **P<0.01; ***P<0.001; ns no significance.

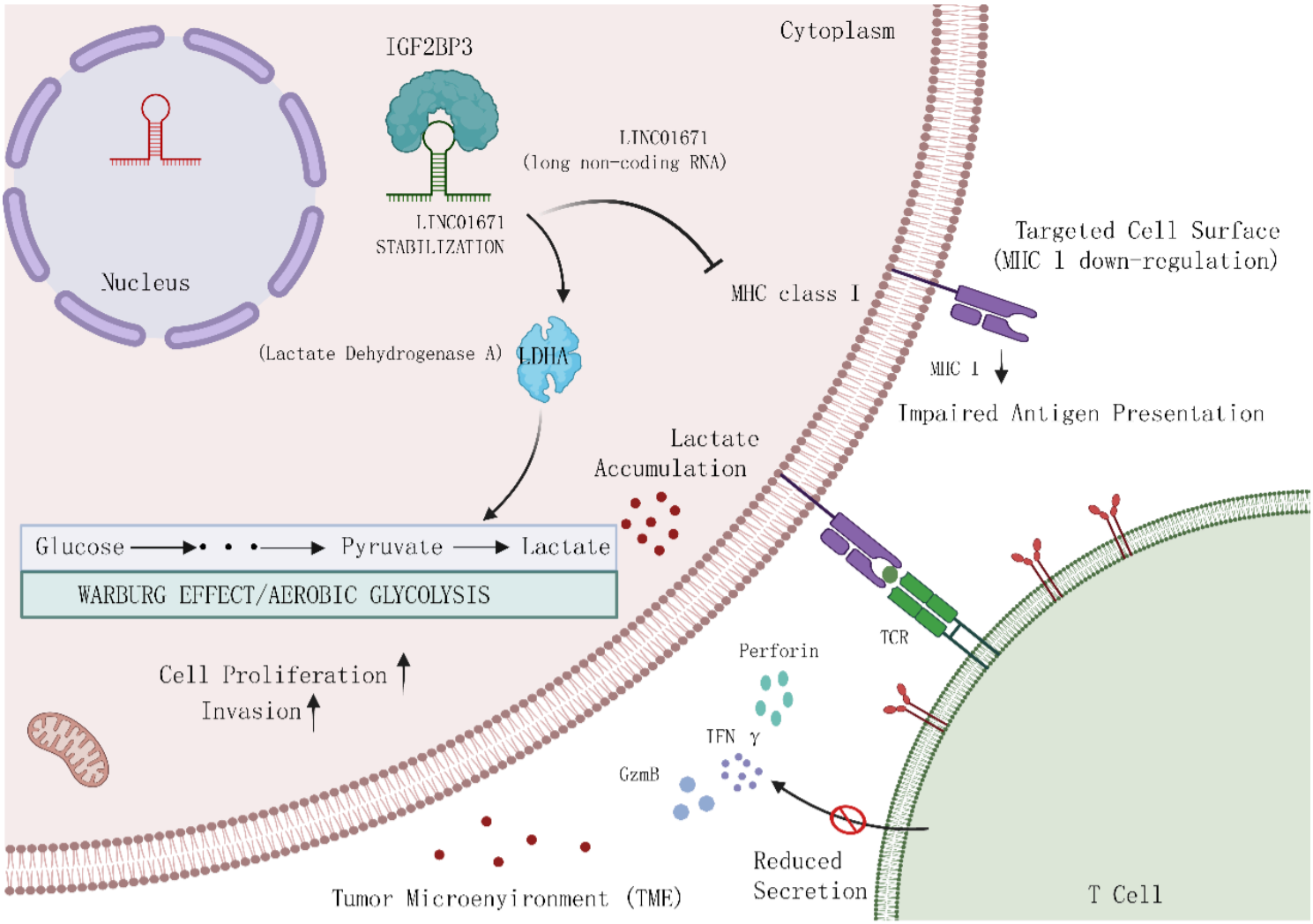


Figure 9

The IGF2BP3/LINC01671/LDHA Axis Drives Metabolic Reprogramming in OCCC

Supplementary Files

This is a list of supplementary files associated with this preprint. Click to download.

- Supplementaryfigures.docx
- SupplementaryTables.xlsx